Measurement of Strange Quark Contributions to the Vector Form Factors of the Proton at Q[superscript 2]=0.22 (GeV/c)[superscript 2]

Measurement of Strange Quark Contributions to the Vector Form Factors of the Proton at $Q^2 = 0.22\ (\mathrm{GeV}/c)^2$

S. Baunack,[1,*] K. Aulenbacher,[1] D. Balaguer Ríos,[1] L. Capozza,[1] J. Diefenbach,[1] B. Gläser,[1] D. von Harrach,[1] Y. Imai,[1] E.-M. Kabuß,[1] R. Kothe,[1] J. H. Lee,[1] H. Merkel,[1] M. C. Mora Espí,[1] U. Müller,[1] E. Schilling,[1] G. Stephan,[1] C. Weinrich,[1] J. Arvieux,[2,†] M. A. El-Yakoubi,[2] R. Frascaria,[2] R. Kunne,[2] F. E. Maas,[2,‡] M. Morlet,[2] S. Ong,[2] J. van de Wiele,[2] S. Kowalski,[3] Y. Prok,[3] and S. Taylor[3]

[1]*Institut für Kernphysik, Johannes Gutenberg-Universität Mainz, J.J. Becherweg 45, D-55099 Mainz, Germany*
[2]*Institut de Physique Nucléaire, CNRS-IN2P3, Université Paris-Sud, F-91406 Orsay Cedex, France*
[3]*Laboratory for Nuclear Science and Department of Physics, MIT, Cambridge, Massachusetts 02139, USA*
(Received 17 November 2008; published 16 April 2009)

A new measurement of the parity violating asymmetry in elastic electron scattering on hydrogen at backward angles and at a four momentum transfer of $Q^2 = 0.22\ (\mathrm{GeV}/c)^2$ is reported here. The measured asymmetry is $A_{\mathrm{LR}} = (-17.23 \pm 0.82_{\mathrm{stat}} \pm 0.89_{\mathrm{syst}}) \times 10^{-6}$. The standard model prediction assuming no strangeness is $A_0 = (-15.87 \pm 1.22) \times 10^{-6}$. In combination with previous results from measurements at forward angles, it is possible to disentangle for the first time the strange form factors at this momentum transfer, $G_E^s = 0.050 \pm 0.038 \pm 0.019$ and $G_M^s = -0.14 \pm 0.11 \pm 0.11$.

DOI: 10.1103/PhysRevLett.102.151803 PACS numbers: 13.40.Gp, 11.30.Er, 12.15.−y, 14.20.Dh

Sea quarks are an important ingredient to describe nucleon properties in terms of fundamental QCD degrees of freedom. Strange quark-antiquark pairs might play a relevant role and affect, e.g., the electromagnetic properties of the nucleon. The contribution of strange quarks to the charge radius and magnetic moment in the nucleon ground state is of specific interest since this is a pure sea quark effect. The strange quark contribution to the electromagnetic form factors of the nucleon can be expressed in terms of the strange electric and magnetic form factors G_E^s and G_M^s. There are various theoretical approaches for estimating the strange form factors [1,2], such as quark soliton models [3–5], chiral quark models [6], quenched lattice calculations [7], or two-component models [8]. Parity violating electron scattering provides a direct experimental approach [9–11].

A measurement of parity violation necessarily involves a weak interaction probe of the nucleon. This provides additional information allowing a measurement of G_E^s and G_M^s. Within the standard model of electroweak interaction, it is known that electromagnetic and weak currents are related. Assuming isospin symmetry, the weak vector form factors $\tilde{G}_{E,M}^p$ of the proton, describing the vector coupling to the Z^0 boson, can be expressed in terms of the electromagnetic nucleon form factors $G_{E,M}^{p,n}$ and the strange form factors $G_{E,M}^s$. The interference between tree level electromagnetic and weak amplitudes leads to a parity violating asymmetry in the elastic scattering cross section of left- and right-handed electrons (LR) σ^L, σ^R: $A_{\mathrm{LR}} = (\sigma^R - \sigma^L)/(\sigma^R + \sigma^L)$. This asymmetry can be written as a sum of three terms, $A_{\mathrm{LR}} = A_V + A_S + A_A$. A_V represents the vector coupling on the proton vertex without strangeness contribution, A_S contains the strange quark vector contribution, and A_A represents the axial coupling to the proton vertex [11]:

$$A_V = -a\rho'_{\mathrm{eq}}\left[(1 - 4\hat{\kappa}'_{\mathrm{eq}}\hat{s}_Z^2) - \frac{\epsilon G_E^p G_E^n + \tau G_M^p G_M^n}{\epsilon (G_E^p)^2 + \tau (G_M^p)^2}\right], \quad (1)$$

$$A_S = a\rho'_{\mathrm{eq}}\frac{\epsilon G_E^p G_E^s + \tau G_M^p G_M^s}{\epsilon (G_E^p)^2 + \tau (G_M^p)^2}, \quad (2)$$

$$A_A = a\frac{(1 - 4\hat{s}_Z^2)\sqrt{1-\epsilon^2}\sqrt{\tau(1+\tau)}G_M^p \tilde{G}_A^p}{\epsilon (G_E^p)^2 + \tau (G_M^p)^2}, \quad (3)$$

with $a = \frac{G_\mu Q^2}{4\pi\alpha\sqrt{2}}$, G_μ the Fermi coupling constant, α the fine structure constant, $\tau = Q^2/(4M_p^2)$, Q^2 the negative squared four momentum transfer, M_p the proton mass, and $\epsilon = [1 + 2(1+\tau)\tan^2\frac{\Theta}{2}]^{-1}$. Θ is the scattering angle in the laboratory frame and $\hat{s}_Z^2(M_Z) = 0.231\,19(14)$ [12] is the square of the sine of the weak-mixing angle. The factors ρ'_{eq} and $\hat{\kappa}'_{\mathrm{eq}}$ include the electroweak radiative corrections evaluated in the minimal subtraction renormalization scheme ($\overline{\mathrm{MS}}$). The electromagnetic form factors $G_{E,M}^{p,n}$ are taken from a Monte Carlo based analysis of the world data [13] resulting in the nonstrangeness expectation $A_0 = A_V + A_A = (-15.87 \pm 1.22) \times 10^{-6}$. The dominant contribution to the uncertainty of A_0 comes from the uncertainty due to the two-quark radiative corrections (anapole moment) in the axial form factor $\tilde{G}_A^p$, followed by the uncertainties in G_M^n and G_M^p.

Recently four groups have published related results. The SAMPLE Collaboration at MIT-Bates [14,15] involved a backward angle measurement on a hydrogen target at a four momentum transfer of $Q^2 = 0.1\ (\mathrm{GeV}/c)^2$ and on deuterium at $Q^2 = 0.1\ (\mathrm{GeV}/c)^2$ and $0.04\ (\mathrm{GeV}/c)^2$, being sensitive mainly to G_M^s and $\tilde{G}_A^p$. The HAPPEX

TABLE I. Average beam parameters $\bar{X}_i$ of the electron beam and the associated false asymmetries $a_i\bar{X}_i$.

i	Parameter	$\bar{X}_i$	$a_i\bar{X}i$
1	Current asymmetry	-0.30 ppm	-0.25 ppm
2	Horizontal position differences	-86.97 nm	$+0.61$ ppm
3	Vertical position differences	-23.84 nm	-0.86 ppm
4	Horizontal angle differences	-8.53 nrad	-0.09 ppm
5	Vertical angle differences	-2.40 nrad	$+0.10$ ppm
6	Energy differences	-0.41 eV	$+0.16$ ppm

Collaboration at TJNAF reported a measurement on a hydrogen target at forward angles at a Q^2 of 0.47 $(\mathrm{GeV}/c)^2$, mainly sensitive to G_E^s [16] and a precise measurement with helium and proton targets at a Q^2 of 0.1 $(\mathrm{GeV}/c)^2$ [17]. Those measurements put tight constraints on the strangeness contribution to the form factors at these momentum transfers. The G0 Collaboration at TJNAF performed a forward angle measurement with several momentum transfers between 0.1 $(\mathrm{GeV}/c)^2$ and 1 $(\mathrm{GeV}/c)^2$, including the momentum transfer discussed here [18]. The A4 Collaboration at MAMI has completed measurements on a hydrogen target at forward angles and momentum transfers of 0.23 $(\mathrm{GeV}/c)^2$ and 0.1 $(\mathrm{GeV}/c)^2$ [19,20]. They were sensitive mainly to G_E^s. Here, a new measurement of the parity violating asymmetry in the elastic scattering of polarized electrons off unpolarized protons at backward angles at $Q^2 = 0.22$ $(\mathrm{GeV}/c)^2$ is presented and the implications of the new result for the strange form factors are discussed. A single measurement of A_S gives a linear combination of G_E^s and G_M^s. Two measurements with the same momentum transfer but with different scattering angles allow the separation of the two strange form factors when $\tilde{G}_A^p$ is taken as an input parameter. With the A4 experimental setup [19,21] at the MAMI accelerator [22] scattering angles Θ either between 30° and 40° or 140° and 150° are possible. As $Q^2 = 4\eta^{-1}E^2\sin^2(\Theta/2)$, where $\eta = 1 + E/M_p(1 - \cos\Theta)$, the momentum transfer can be selected by varying the beam energy E. To match the Q^2 value of the A4 forward measurement a beam energy of 315.1 MeV was chosen for the backward angle experiment.

The experimental setup was described in detail in [19]. Here we summarize the basic components and emphasize the modifications that have been made. A superlattice photocathode delivered a polarized electron beam with an intensity of 20 μA and an average polarization P_e of about 70%. The beam polarization was measured once a week using a Møller polarimeter with a precision of 2%. In addition, a Mott and a transmission Compton polarimeter were used. Altogether, the uncertainty to the beam polarization is 4%. It was important to minimize helicity correlated beam fluctuations in position, angle, current, and energy that introduce false asymmetries due to changes in luminosity, cross section, or solid angle. Table I lists the measured beam parameters during the 1100 h of asymmetry data taking. The liquid hydrogen target [23] was 23.4 cm long yielding a luminosity $L \approx 1.2 \times 10^{38}$ cm^{-2} s^{-1}. Target density fluctuations were monitored by Cherenkov luminosity monitors located at small scattering angles [24] and were kept below $\Delta L/L < 10^{-6}$ averaged over the whole data set. The scattered electrons were detected in a homogenous electromagnetic calorimeter that consists of 1022 lead fluoride (PbF_2) crystals [25] as single events achieving an energy resolution of about $3.9\%/\sqrt{E}$. The detector covered a solid angle of $\Delta\Omega = 0.62$ sr.

The most important aspect of the backward measurement is the installation of 72 plastic scintillators in front of the PbF_2 crystals (see Fig. 1). Used in coincidence with the calorimeter, they enable the separation of charged from neutral particles. Photons from π^0 decay could thus be separated from scattered electrons. The energy that was deposited by a particle in the calorimeter was digitized by an 8 bit ADC and stored into a coincidence or a noncoincidence histogram depending on the trigger signal

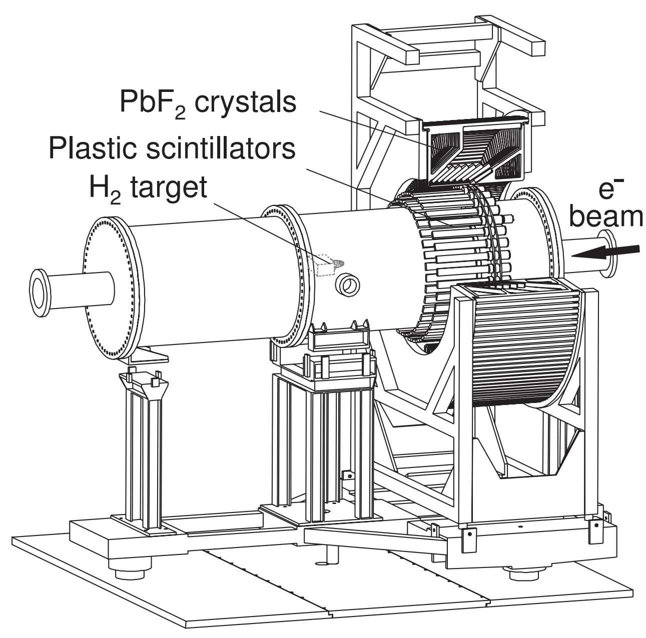

FIG. 1. Drawing of the PbF_2 calorimeter. The scintillators are placed between the scattering chamber and the lead fluoride crystals. The system is mounted on a rotatable platform.

from the scintillator. Furthermore a polarization signal distinguished between the two helicity states of the beam. Altogether each calorimeter channel produced four histograms for each 5 min data taking run.

The data analysis was similar to that of the previous measurements [20]. Modifications were needed since the coincidence histograms were polluted by high energy photons converting into e^+e^- pairs in the aluminum wall of the vacuum chamber and in the scintillator. The LR asymmetry of the γ background was determined from the noncoincidence spectra. A detailed Monte Carlo simulation using GEANT4 was implemented for tracking shower particles and calculating the detector response. The simulation reproduced the measured spectrum well for energies above 125 MeV, while for lower energies threshold effects of the analogue readout electronics become important. From the simulation one can derive as a function of the γ energy both the probability of a γ to convert and trigger the scintillator and the mean energy loss of the generated e^+e^- pairs. Figure 2 shows the measured energy spectra and the contributions from the different processes. The contribution to the background arising from aluminum events from the target entrance and exit windows was determined by a measurement with an empty target and is about 4.5%. The background elimination was achieved by scaling the measured noncoincidence spectra with the conversion probability and shifting them by the energy loss. Different methods for this procedure were applied and gave differences in the final asymmetry below 0.2×10^{-6}.

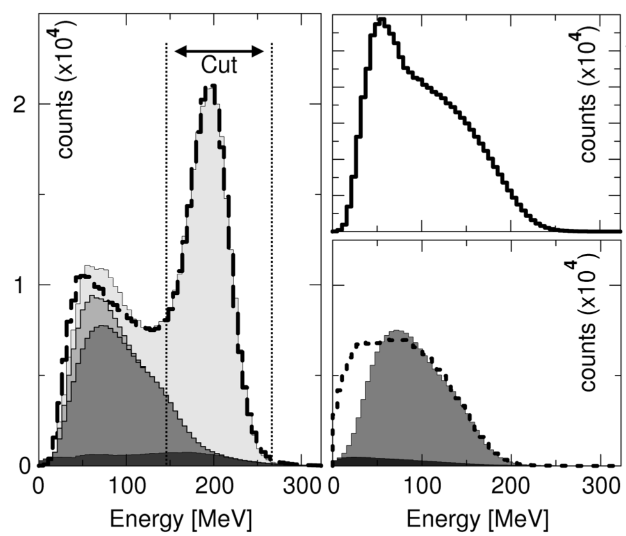

FIG. 2. Left panel: The measured energy spectrum of coincidence events is shown by the dashed line. One can clearly identify the peak of the elastic scattered electrons. The contributions of the different processes are shown from bright to dark: (i) the elastically scattered electrons, (ii) the inelastically scattered electrons, (iii) the converted photons from π^0 decay, and (iv) empty target background. Upper right panel: The solid line shows a measured energy spectrum of noncoincidence events. Lower right panel: The dotted line shows the background contribution to the coincidence spectrum estimated from the noncoincidence events by applying the shifting and scaling method in comparison with the photon background obtained from the simulation (gray) together with the shifted and scaled noncoincidence events from an empty target measurement (dark).

The number of elastic events for the two helicities was determined by applying cuts on the coincidence energy histograms as indicated in Fig. 2 by the dotted lines and summing up all 730 channels of the inner five calorimeter rings. For each run the raw asymmetry is calculated. The false asymmetries are corrected using the ansatz $A_{\mathrm{raw}} = A_{\mathrm{expt}} + \sum_{i=1}^{6} a_i X_i$, where the X_i denote the helicity correlated beam parameters as defined in Table I. The a_i denote the correlation coefficients between the observed asymmetry A_{raw} and the beam parameters X_i. These coefficients have been determined from geometry and in addition from the intrinsic beam fluctuations via a multiple linear regression analysis. Both methods yield only small corrections relative to the measured asymmetry and agree within the statistical precision. Finally the physical asymmetry A_{LR} is obtained by normalization of A_{expt} by the electron beam polarization P_e: $A_{\mathrm{LR}} = A_{\mathrm{expt}}/P_e$. About half of our data was taken with a half-wave plate inserted in the laser optics of the electron source. This leads to a reversal of the beam helicity and a partial compensation of helicity correlated false asymmetries. All relevant corrections applied to the measured asymmetry are listed in Table II. The asymmetry for the aluminum events is calculated in the static approximation. Another source of background is accidental coincidence events in the scintillators with a fraction of about 1.3%. Since the event rate on the detector is 4–8 times smaller than in our forward measurements, corrections on the asymmetry due to pileup are negligible here. Figure 3 shows the parity violating asymmetries for the whole data set. The sign flip when the half-wave plate was inserted can be clearly observed. In total 3×10^{12} coincidence events were used for the full analysis. An asymmetry of $A_{\mathrm{LR}} = (-17.23 \pm 0.82_{\mathrm{stat}} \pm 0.89_{\mathrm{syst}}) \times 10^{-6}$ is extracted.

From the difference between A_{LR} and A_0 the linear combination of the strange electric and magnetic form factors $G_M^s + 0.26 G_E^s = -0.12 \pm 0.11 \pm 0.11$ is obtained, where the first error comes from the measurement and the

TABLE II. Applied corrections to the measured asymmetry and their contribution to the systematic error.

Applied scaling factor	Scaling factor	Error
Polarization P_e	0.683	0.040

Applied corrections	Correction (ppm)	Error (ppm)
Helicity correlated beam differences	0.14	0.39
Accidental coincidence events	−0.19	0.02
Al windows (H_2 target)	0.29	0.04
Dilution of π^0 decay photons	−1.49	0.28

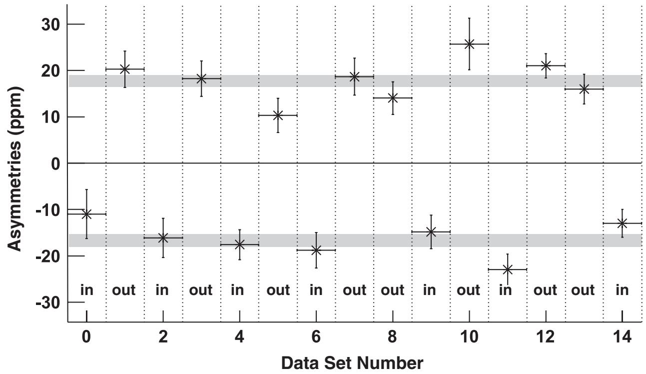

FIG. 3. Measured asymmetries A_{LR} with respect to the position of the half-wave plate at the electron source (in or out). The reversal of the helicity can be easily observed in the sign flip of the extracted asymmetries. The two gray bands show fits to the data, $A_{\mathrm{out}} = (17.70 \pm 1.27)$ ppm and $A_{\mathrm{in}} = (-16.68 \pm 1.37)$ ppm (omitting systematic errors).

second from the uncertainty in the axial and electromagnetic form factors of the nucleon. In Fig. 4 the shaded band shows the possible values of G_E^s and G_M^s within the one-σ uncertainty. The hatched band shows the A4 result of the forward angle measurement at the same momentum transfer. Because of a careful reanalysis of the electron polarization measurement and using an up-to-date parametrization of the electromagnetic form factors [13], the value of the linear combination has shifted down from $G_E^s + 0.225G_M^s = 0.039 \pm 0.028 \pm 0.020$ as presented in [19] to $G_E^s + 0.224G_M^s = 0.020 \pm 0.029 \pm 0.016$. Disentangling the linear combinations, one gets $G_E^s = 0.050 \pm 0.038 \pm 0.019$ and $G_M^s = -0.14 \pm 0.11 \pm 0.11$. Including the G0 forward angle measurement at $Q^2 = 0.23$ (GeV/c)^2 one gets a more precise value of $G_E^s = 0.035 \pm 0.030 \pm 0.019$. The strange form factors presented here are determined simultaneously from two complementary A4 measurements with the same momentum transfer using the same method. In contrast to the only existing published backward angle measurement at a lower Q^2 of 0.1 (GeV/c)^2 favoring a positive value of G_M^s [14], the new result favors a negative strange magnetic moment as predicted by many models and also in accordance with the latest lattice calculation [7]. Furthermore, it disfavors a negative G_E^s in this momentum transfer region as suggested by [18]. Both HAPPEX and A4 Collaborations have scheduled measurements in the near future to clarify the situation for G_E^s at $Q^2 = 0.6$ (GeV/c)^2.

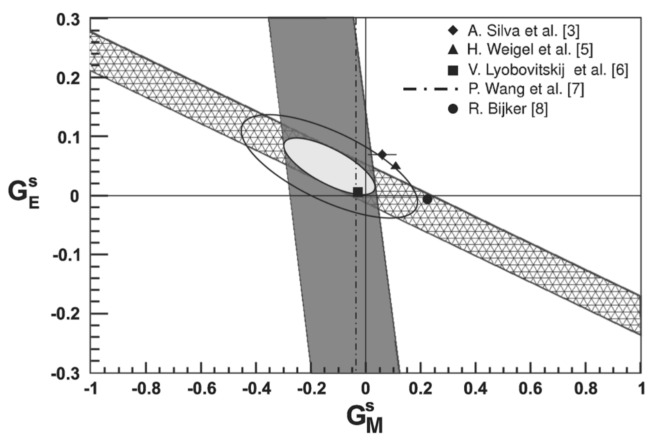

FIG. 4. The linear combination of $G_E^s + \zeta G_M^s$ from this work (solid band) together with the A4 forward angle measurement [19] (hatched band). The bands represent the possible values of $G_E^s + \zeta G_M^s$ within the one-σ uncertainty with statistical and systematic error added in quadrature. The ellipses show the 68% and 95% C.L. constraints in the G_E^s-G_M^s plane. Also shown are theoretical predictions [3,5–8].

*Corresponding author.
baunack@kph.uni-mainz.de
†Deceased.
‡Present address: Gesellschaft für Schwerionenforschung Darmstadt and Johannes Gutenberg-Universität Mainz, Germany.

[1] Special issue on ''Parity violation and hadronic structure,'' edited by S. Kox *et al.* [Eur. Phys. J. A **24**, Suppl. 2, 1 (2005)].
[2] *Proceedings of 3rd Workshop on Parity Violation PAVI 2006, Milos, June 2006*, edited by S. Kox *et al.* (SIF and Springer-Verlag, Berlin, Heidelberg, 2007).
[3] A. Silva, H. C. Kim, D. Urbano, and K. Goeke, Phys. Rev. D **74**, 054011 (2006).
[4] K. Goeke *et al.*, Eur. Phys. J. A **32**, 393 (2007).
[5] H. Weigel *et al.*, Phys. Lett. B **353**, 20 (1995).
[6] V. E. Lyubovitskij, P. Wang, T. Gutsche, and A. Faessler, Phys. Rev. C **66**, 055204 (2002).
[7] P. Wang, D. B. Leinweber, A. W. Thomas, and R. D. Young, arXiv:0807.0944.
[8] R. Bijker, J. Phys. G **32**, L49 (2006).
[9] B. Kaplan and A. Manohar, Nucl. Phys. **B310**, 527 (1988).
[10] D. H. Beck and B. R. Holstein, Int. J. Mod. Phys. E **10**, 1 (2001).
[11] M. J. Musolf *et al.*, Phys. Rep. **239**, 1 (1994).
[12] C. Amsler *et al.*, Phys. Lett. B **667**, 103 (2008).
[13] M. A. El-Yakoubi *et al.*, in *Proceedings of 3rd Workshop on Parity Violation PAVI 2006, Milos, June 2006* (Ref. [2]), p. 119.
[14] D. T. Spayde *et al.*, Phys. Lett. B **583**, 79 (2004).
[15] T. M. Ito *et al.*, Phys. Rev. Lett. **92**, 102003 (2004).
[16] K. A. Aniol *et al.*, Phys. Lett. B **509**, 211 (2001).
[17] A. Acha *et al.*, Phys. Rev. Lett. **98**, 032301 (2007).
[18] D. Armstrong *et al.*, Phys. Rev. Lett. **95**, 092001 (2005).
[19] F. E. Maas *et al.*, Phys. Rev. Lett. **93**, 022002 (2004).
[20] F. E. Maas *et al.*, Phys. Rev. Lett. **94**, 152001 (2005).
[21] F. E. Maas *et al.*, Eur. Phys. J. A **17**, 339 (2003).
[22] A. Jankowiak, Eur. Phys. J. A **28**, Suppl. 1, 149 (2006).
[23] I. Altarev *et al.*, Nucl. Instrum. Methods Phys. Res., Sect. A **564**, 13 (2006).
[24] Th. Hammel *et al.*, Nucl. Instrum. Methods Phys. Res., Sect. A **564**, 1 (2006).
[25] P. Achenbach *et al.*, Nucl. Instrum. Methods Phys. Res., Sect. A **465**, 318 (2001).